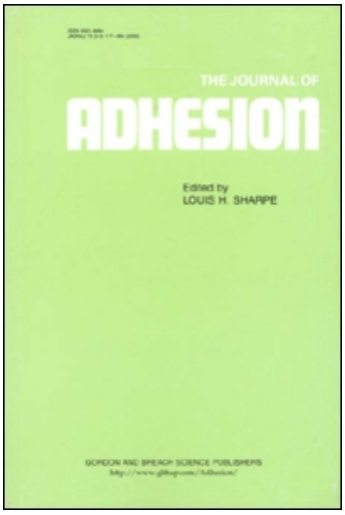


**The Journal of Adhesion**
Publication details, including instructions for authors and subscription information:
http://www.informaworld.com/smpp/title~content=t713453635

# Elastic Properties of an Epoxy - Aluminum Interphase Measured Using an Acoustic Microscope

V. Safavi Ardebili[a]; A. N. Sinclair[a]; J. K. Spelt[a]
[a] Department of Mechanical and Industrial Engineering, University of Toronto, Canada

**To cite this Article** Ardebili, V. Safavi , Sinclair, A. N. and Spelt, J. K.(2000) 'Elastic Properties of an Epoxy - Aluminum Interphase Measured Using an Acoustic Microscope', The Journal of Adhesion, 73: 4, 385 — 416
**To link to this Article: DOI:** 10.1080/00218460008029587
**URL:** http://dx.doi.org/10.1080/00218460008029587

J. Adhesion, 2000, Vol. 73, pp. 385–416
Reprints available directly from the publisher
Photocopying permitted by license only



# Elastic Properties of an Epoxy–Aluminum Interphase Measured Using an Acoustic Microscope

V. SAFAVI ARDEBILI, A. N. SINCLAIR* and J. K. SPELT

*Department of Mechanical and Industrial Engineering, University of Toronto, Canada, M5S 3G8*

*(Received 29 June 1999; In final form 4 April 2000)*



The interphase region in an epoxy–aluminum adhesive bond has been micromechanically characterized using a new acoustic microscope which employs a coupling fluid with a low speed of sound. A $V(z)$ curve fitting method was used to calculate the property profiles across the interphase. The interphase region appeared to have shear and longitudinal wave speeds which were, on average, 14% and 11% larger than those of the bulk adhesive, respectively. The average interphase density was 5.5% smaller than the bulk density. The results were in conformity with a previous microscopic and nano-indentation study on the same adhesive system.

*Keywords*: Adhesive; Interphase; Epoxy; Acoustic microscope; Micromechanics

## 1. INTRODUCTION

The concept of a region adjacent to the interface within the adhesive layer, with different properties from the bulk adhesive, has existed for a considerable time [1]. This layer has been called the weak boundary layer, but more recent studies in metal-to-metal adhesive joints refer to it as an "interphase" (Fig. 1) [2]. In a typical epoxy–aluminum joint, an oxide layer with varying degrees of complexity might be present at the surface of the adherend. The interphase can have a variable thickness

*Corresponding author. Tel.: 416-978-3051, Fax: 416-978-7753, e-mail: sinclai@mie.utoronto.ca

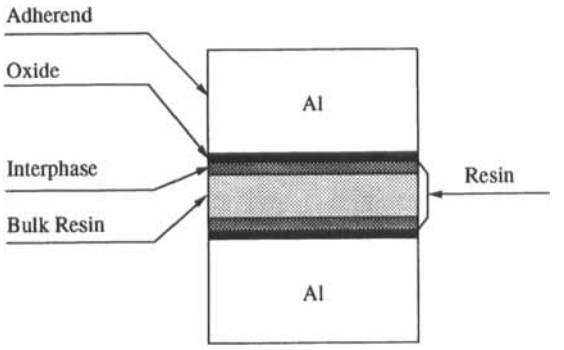


FIGURE 1 A schematic section through an adhesive joint.

and both the interphase and the bulk resin can be heterogeneous. There exists no general agreement on the nature of the interphase, its thickness, mechanism of formation, or its relationship to the durability of a joint. This lack of agreement is the result of two factors: First, only a few direct studies of the interphase and its structure in adhesive joints have been published. Second, the interactions leading to the formation of the interphase are complicated and system specific, such that it is often impractical to draw general conclusions.

The present work formed part of an effort to use ultrasonic nondestructive evaluation as a means of monitoring environmental degradation in epoxy–aluminum adhesive joints. Interphase elastic constants are needed in order to construct multilayer models of ultrasonic wave propagation in an adhesive joint. Here, a first attempt has been made to measure ultrasonically the elastic properties in HYSOL EA9346 adhesive as a function of depth, beginning from the aluminum surface (AA1100 alloy) and ending at the bulk adhesive.

One of the earliest studies of the interphase was by Cuthrell [3], who found that several unfilled (without inorganic particles), untoughened (not containing rubber particles) epoxy resins, which were molded either in metal or polytetrafluoroethyene, displayed an interphase. This interphase consisted of "floccules" of polymer surrounded by resin-like channels of a different structure. The size and depth of this structure were much larger than that normally anticipated in adhesive joints; *i.e.*, the interfacial region could extend from the mold wall several hundred microns into the bulk resin.

In a set of fiber pull-out experiments in an electron microscope, Williams *et al.* [4] observed a soft interphase (in comparison with the bulk epoxy resin). The carbon fibers were either oxidized or coated with an adhesion-promoting commercial size. When carbon fibers were coated with a phenolic resin, the interphase was absent. Using single-filament fragmentation tests as a function of temperature, Skourlis and McCullough [5] found that the critical aspect ratio of fragments indicated the existence of an interphase having a glass transition temperature less than that of the bulk resin. Al-Moussawi *et al.* [6] measured the properties of a synthetic interphase formed by mixing an epoxy matrix with different amounts of silanesizing. They found that the mixture's properties were quite different from the pure epoxy, having a lower glass transition temperature, a higher modulus, greater tensile strength, and lower toughness.

Possart [7] measured a distribution of negative charge up to a depth of 10 microns from the interface between low density polyethylene and aluminum. Additional evidence of uneven charge distribution was found by Cognard [8] by virtue of electrical conduction through the joint thickness in 10–20 μm thick adhesive joints. This was attributed to conductive channels inside the adhesive interphase where the charge concentration is high. It was concluded that, if the joint was sufficiently thin, the charged resin channels originating from both surfaces could merge and enable electrical conduction. It was proposed that the column structure observed by Hahn and Koetting [9] might be similar to the structure observed by Cuthrell [3].

Crompton [10] used transmission electron microscopy of ultramicrotomed joint sections, cut normal to the interface, to reveal two types of interphase in an epoxy–aluminum system. The interphase showed a difference in electron transparency over a distance of approximately 1 μm from the aluminum as compared with the bulk and contained a second distinctive region in the first 10 nm of resin adjacent to the interface. The boundary between the interphase and the bulk resin was highly irregular. The interphase also seemed to contain, on average, less fumed silica than the bulk, although a more pronounced characteristic was associated with differences in the polymer structure between the bulk and the interphase leading to the observed variations in electron transparency. Nevertheless, Crompton found only minor differences in the chemical bonds between the two regions [11].

Spigel and Roy [12] measured the *in situ* shear modulus of a structural adhesive using a sandwich beam loaded in 3-point bending, in which the adhesive was constrained as a thin layer. The measured bulk shear modulus was up to an order of magnitude lower than the bulk shear modulus as traditionally determined from a tensile test. Their finite element model did not include the presence of any interphase in the adhesive layer; however, the authors suggested that the observed low modulus was a result of bond imperfections at the steel–epoxy interface, as seen in their microscope studies. Ramakrishnan *et al.* [13] observed a reduction in the dynamic Young's modulus of an epoxy adhesive as the thickness of the bond-line was increased from 48 μm to 466 μm. They did not report any of the adherend materials or surface pretreatment procedures used in their work.

Nakamae *et al.* [14] observed a preferential adsorption of 4,4-diaminodiphenylmethane (DDM) onto the aluminum oxide. This localization of the curing agents at the aluminum surface can be a possible mechanism for the difference between the polymer structure in the bulk adhesive and the interphase of epoxy–aluminum systems. Affrosman *et al.* [15] made similar observations.

Using high-surface-area carbon black as the model surface, Wang and Garton [16] showed the importance of interfacial reactions for difunctional epoxy resins cured with either anhydrides or aromatic amines. Adsorption and catalytic effects produced a reduction in the cross-link density of the interphase.

Maguire *et al.* [17] discussed the origin of the interphase and its thickness, which ranges over several orders of magnitude; *i.e.*, a few Angstroms up to several microns. They considered the fundamental question of how small-scale phenomena (nanometer range) can result in interphases up to several micrometers thick. They reviewed the molecular dynamic simulations and related studies, and demonstrated the possibility of the formation of a thick interphase (of thickness in the micron range) by introducing non-linearity in their model calculations.

Knollman [18] measured shear modulus variations in two epoxy adhesives near an aluminum interface. He determined the Rayleigh critical angle in a conventional pitch–catch ultrasonic test rig at 25 MHz using a coupling fluid with a low speed of sound. The samples

were produced by vacuum casting an epoxy resin on FPL-etched aluminum substrates. The shear modulus increased from 1.9 GPa to 2.5 GPa as the distance from the aluminum increased from 100 μm to 400 μm. The extent of the interphase was increased by longer epoxy cure times.

Cognard [19] used an acoustic microscope at 1.3 GHz with water couplant to image the interphase between a 0.1 μm thick gold foil and two types of epoxy. He observed an interfacial cellular structure which was estimated to extend 3–4 μm from the gold surface into the epoxy and had an average cell diameter of approximately 15–30 μm. The imaging was performed through the gold foil, but no micromechanical characterization was done on the interphase and no explanation was proposed for the observed contrast between the various phases in the cellular microstructure.

Verma *et al.* [20] studied normal-to-fiber sections through various types of carbon-fiber-reinforced polymer composites by imaging the sections with a conventional acoustic microscope operating at 1 GHz. Rayleigh waves were excited inside the stiff carbon fibers, but only lateral compressional waves were excited inside the matrix. The reflected lateral compressional waves from the matrix-fiber interface resulted in interference fringes around the fibers in the images. A plot of the normalized intensity of these fringes as a function of radial distance from the fiber was used to characterize the interface. The differences in the curves of various specimens were mistakenly attributed to the degree of interfacial coupling (The curves were already normalized and the reflection coefficient information was lost). No reference to the interphase was made in this work, but one can suggest that the specimen-to-specimen differences in the fringe intensity–radial distance curves were likely due to the differences in the mechanical properties of the propagation medium adjacent to the fiber-matrix interface, *i.e.*, the interphase.

Sklar and Briggs [21] performed acoustic microscope $V(z)$ measurements on 0.2 μm thick oxide layers on aluminum substrates, as well as 0.2 μm and 1 μm thick spin-coated polymethylmethacrylate (PMMA) layers on either polished aluminum or phosphoric acid anodized oxide layers. The acoustic microscope probes used in this work had frequencies up to 980 MHz and used water as the coupling fluid. They found that the large attenuation in the PMMA layer did not

prevent high-frequency measurements; however, the interpretation of the results was complicated by the intricate morphology of anodized oxide layers.

The present authors [22] characterized the interphase in an epoxy–aluminum system using scanning electron microscopy, ion etching, energy-dispersive X-ray analysis, and nano-indentation. The interphase was of irregular thickness, nominally between 2 and 6 μm, and corresponded to a region of greater resistance to ion etching and a marked absence of the silica particles used in the epoxy adhesive. Their nano-indentation tests, traversing various sections of the interphase from the aluminum to the bulk resin, showed that the interphase region had, on average, an effective elastic modulus ($E/(1-\nu^2)$) that was 13% greater than that of the bulk resin, located far from the aluminum.

In all of the previous studies of plastics using acoustic microscopes, the speed of sound in the coupling fluid was not small enough for launching Rayleigh surface waves on the plastics; therefore, it has not been possible to obtain the standard $V(z)$ curve that can be used to derive elastic properties of the surface layer. In the present work, a new acoustic microscope [23], which was capable of launching Rayleigh waves on the surface of plastics, was used to characterize the interphase of the epoxy HYSOL EA9346 in an adhesive joint made with aluminum AA1100 alloy. This device made use of a new coupling fluid, HCFC-225 da, with a very low speed of sound and a moderate sound attenuation factor [24]. The characterization was made on small specimens cut from the adhesive joint. Each specimen was sectioned in order to expose the interphase at various distances from the adherend's surface. Several $V(z)$ curves were collected on each specimen and the elastic properties were then calculated by an optimization method.



## 2. SPECIMEN PREPARATION

All of the specimens were cut from a pair of identical sample joints, made using 10 mm thick AA1100 alloy as the main adherend and AA7075-T6 as the dummy adherend (Fig. 2). AA1100 is a relatively

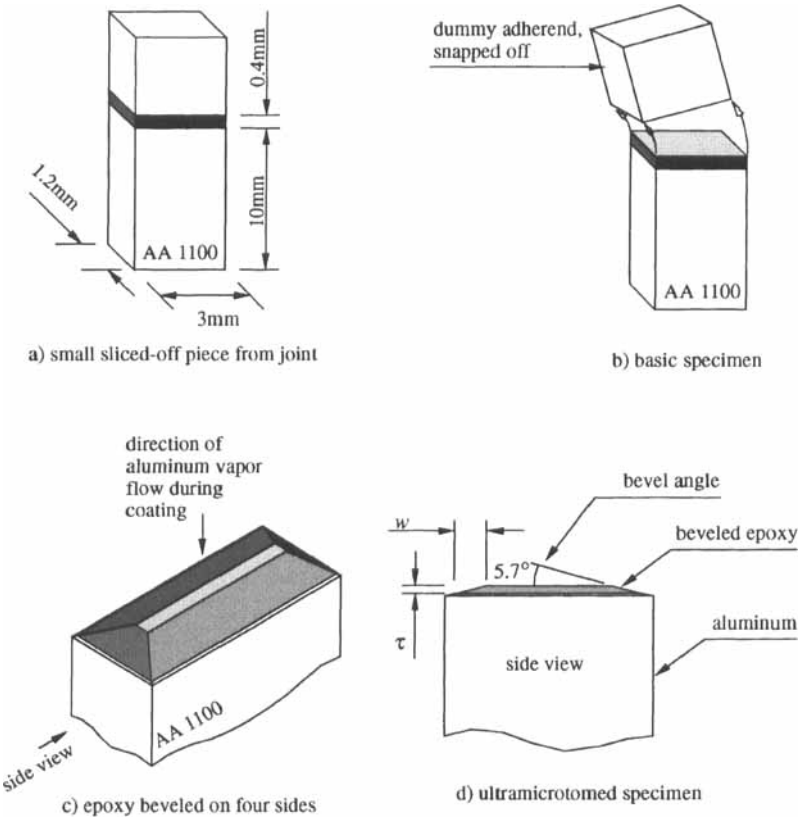


FIGURE 2 Specimen preparation for acoustic microscopy: (a) A small sliced-off piece from the sample joint. (b) With the dummy adherend snapped off, the specimen was ultramicrotomed. (c) Perspective view of the specimen with the four sides beveled. (d) Side view after removing most of the epoxy. The width, $w$, of the remaining beveled epoxy is directly related to the thickness, $\tau$.

soft alloy which facilitated the cutting of ultramicrotome sections using a glass knife. The dummy adherend only served to ease handling, and its interphase was not part of this study.

Prior to adhesive application, the AA1100 adherend was polished using a sequence of abrasive papers of up to 600 mesh, then using a 5 μm polycrystalline diamond suspension on a hard pad to retain flatness. Next, a 1 μm polycrystalline diamond suspension was used on a soft pad, followed by a 0.05 μm alumina suspension. The surface of

the AA1100 adherend was then chemically pretreated using a standard FPL etching procedure [25]. The dummy adherend was not chemically pretreated to ease its removal prior to the ultramicrotomy.

The adherend surface pretreatment was chosen such that a very thin oxide layer (less than 100 nm thick) would develop on the surface. A thin oxide layer was essential for avoiding complications in the interpretation of the acoustic microscope measurements. A micron-thick oxide layer, such as the oxide associated with anodization pretreatments, could significantly interact with the ultrasonic waves, making the extraction of the interphase properties from the ultrasonic experimental data even more difficult.

After the aluminum had been pretreated, it was warmed to between 40°C and 50°C to ease the spreading of the adhesive and reduce the incidence of voids. The adhesive was the single-part paste epoxy, HYSOL EA-9346 (Hysol Aerospace Prods., Pittsburgh, CA, USA), which contains 1 to 5% (by weight) hydrophobic $SiO_2$ particles. Bondline thickness was controlled at 0.4 mm using Teflon® shims, and the adhesive was cured at a temperature of 120°C for one hour.



As depicted in Figure 2, a small piece was cut from the sample joint and the dummy adherend was snapped off the specimen. Next, the four sides of the exposed epoxy layer were beveled such that a thin margin of aluminum substrate was exposed all around the epoxy. This beveled shape served two purposes: first, it guaranteed a full encapsulation of the epoxy under a 50 nm aluminum coating as explained later; second, the thickness of the remaining epoxy, $\tau$, could be estimated by measuring the width of the bevel, $w$, on the long side of the specimen. After beveling, most of the epoxy was removed by cutting thin slices parallel to the adherend–adhesive interface until the desired thickness was reached. A bevel angle of 5.7° resulted in a $w/\tau$ ratio of 10. This angle could be set to within $\pm 0.2°$ in the ultramicrotome and the bevel width could be measured to $\pm 2\,\mu m$. The resulting uncertainty in the measured resin thickness, $\tau$, was $\pm 0.4\,\mu m$ for $\tau = 2\,\mu m$, and $\pm 1\,\mu m$ for $\tau = 10\,\mu m$. Another source of uncertainty in the resin thickness was deviations of the glass knife edge from a straight line (this source of uncertainty can be eliminated by the use of a diamond knife). However, the thickness of resin was determined more accurately by destructive sectioning through the specimen after acoustic microscopy. Eleven specimens were

prepared, covering a range of epoxy thickness from 3 to 40 μm. For thicknesses larger than 22 μm, the nominal bevel angle was increased to 11.3°.

A glass knife was used for the ultramicrotomy. In order to produce a smooth surface finish, the thickness of the last few slices of each specimen was reduced to less than 1 μm, and these cuts were performed using a fresh knife. A surface roughness of $Ra = 0.038$ μm could easily be achieved. Compared with the wavelength of sound at 250 MHz in the coupling fluid (~3 μm), these values of roughness would not have a significant effect on the ultrasonic measurements.

A concern in the acoustic microscopy of plastics is the absorption of the couplant by the specimen. Couplant absorption can alter the measured properties or damage the polymer surface. In order to prevent this, a diffusion barrier was applied by thermally evaporating pure aluminum ($> 99.99\%$) onto the specimens in an ultrahigh-vacuum chamber. The thickness of the coating was controlled by measuring the amount of aluminum which was loaded into the deposition instrument's crucible. In order to find the correct amount of aluminum, several test runs were performed on masked pieces of microscope slide, where the thickness of the deposited aluminum could be measured independently using a surface profilometer. Specimens were retained in a desiccator prior to the coating operation and were held in the ultrahigh-vacuum device for more than 48 hours before coating to minimize the outgassing from the epoxy during deposition. A masked microscope slide was coated along with the specimens as a control piece, and the actual deposited thickness was measured later. An intended deposition thickness of 50 nm resulted in a typical deposited average thickness of 53 nm.



## 3. ACOUSTIC MICROSCOPY

Acoustic microscopy involves the measurement of reflected ultrasonic wave amplitude and phase, $V$, as a function of the relative displacement, $z$, between the acoustic lens and the surface of the specimen. In the present experiments, a typical $V(z)$ acquisition would require approximately 20 minutes. Scans were performed over a $z$ range of 80 to 100 μm, and 160 to 200 data points were collected at

equidistant $z$ values. Both voltage and phase of the probe response were recorded in these measurements, and 12 $V(z)$ curves were collected at randomly distributed sites on the surface of each of the eleven specimens, such that each collection site was 50 – 100 μm from its nearest neighbor.[1]

The twelve $V(z)$ curves for each of the eleven specimens were averaged at each $z$ value, and the resulting eleven averaged $V(z)$ curves were analyzed in order to estimate the interphase property profiles as a function of distance from the aluminum – adhesive interface. The problem was of a variational nature: to find functions for the property distributions which resulted in the best fit between the calculated and the experimental $V(z)$ curves. This problem of depth profiling by acoustic microscopy has never been addressed in the literature before, and an exact solution to the inverse problem of the calculation of a property profile from numerous $V(z)$ curves (collected at various depths) remains unsolved. (The case of a homogeneous layer on a substrate has been handled by fitting the forward solution with the experimental data [27 – 28].)

It was assumed that the epoxy is an isotropic material in both the bulk and the interphase. A preliminary investigation of the EA 9346 epoxy at the bulk and interphase by X-ray spectrometry showed no ordered structures; this helped to justify the assumption of isotropy [26]. This assumption reduced the number of the property functions to five; *i.e.*, the speed of the longitudinal wave, $\nu_l$, the speed of the shear wave, $\nu_s$, the attenuation factor for longitudinal wave, $\alpha_l$, the attenuation factor for shear wave, $\alpha_s$, and the density, $\rho$. It was also assumed that the aluminum substrate is isotropic and values from literature were used for its elastic properties. Although a single crystal of aluminum is slightly anisotropic and a $V(z)$ acquisition site could fall entirely within a single grain of the adherend, these minor effects could be minimized by averaging multiple $V(z)$ curves on a single specimen. Finally, it was assumed that the elastic properties and density of the Al diffusion barrier coating were equal to that of the bulk aluminum. Since this layer had only a small perturbing effect on

[1] The operating frequency of this acoustic microscope was 250 MHz resulting in a Rayleigh wave probing depth of approximately 4.5 μm on epoxy. The coupling fluid was HCFC-225 da which has a compression wave velocity of 663 m/s, and an attenuation factor of 117 dB/mm at 250 MHz and 28°C [26].

the shape of the $V(z)$ curve, the bulk aluminum properties were an adequate approximation for the purpose of these calculations.

A data reduction scheme was developed to determine material properties of the interphase, such that the experimental $V(z)$ curves would match those calculated numerically. Details are presented in Appendix I. The key steps to this scheme were as follows:

- The ultrasonic reflectance function, $R(\theta)$, was determined for each specimen.
- The lens of the acoustic microscope was calibrated by determining the pupil function of the lens.
- The depth profiles of material properties of the interphase were discretized in order to facilitate numerical calculations. The continuous property profiles could then be approximated by linear interpolation between these reference or "defining points", selected through the interphase (Fig. 3).
- An objective function, $U$, was selected that represented a measure of the difference between the experimental and calculated $V(z)$ curves for the eleven specimens.
- An iterative scheme was developed to adjust the interphase material property values to yield a minimum value for $U$.

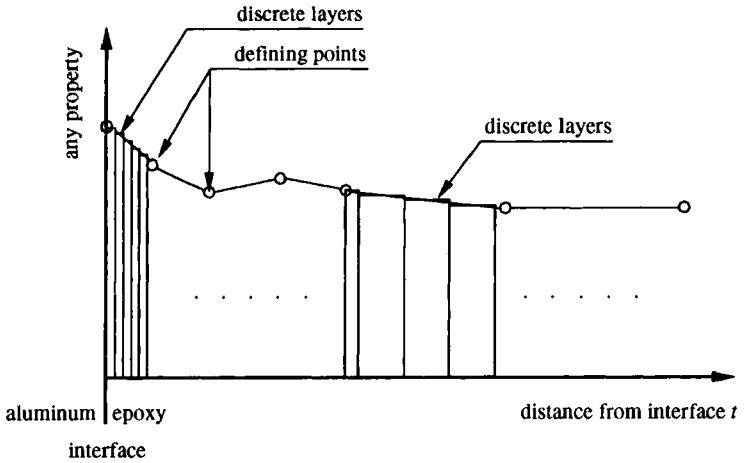


FIGURE 3 Property function defining points and discretization of the interphase into a multilayer medium.

Although discretization of the material property profiles led to the creation of a large number of adjustable parameters, the solution algorithm was stable. In a series of sensitivity studies it was found that the calculated $V(z)$ curves were perturbed in a minor, predictable manner corresponding to small adjustments in material properties of the interphase. In addition, it was found that no satisfactory agreement could be reached between calculated and experimental profiles without inclusion of an interphase layer in the numerical work. The effect of the aluminum substrate was explicitly included in the calculation of the $V(z)$ curves, such that no artifacts originated from waves reflecting from the aluminum, nor from the aluminum causing localized constraint of the adjacent epoxy.

## 4. RESULTS

### 4.1. *V(z)* Curves

The eleven experimental $V_e(z)$ curves are presented as dotted lines in Figure 4. Each curve is the average of 12 $V(z)$ profiles, each collected at a different point on one specimen. Generally the shapes of the $V_e(z)$ curves were more repeatable for the specimens with a relatively large epoxy thickness, $\tau$ (greater than about 10 μm). Calculations of $V_t(z)$ showed that a specimen with small epoxy thickness, $\tau$, had a relatively large sensitivity to the exact thickness value. It should be noted that attaining a high degree of fractional uniformity of the thickness (magnitude of local variations in $\tau$ divided by average $\tau$) was the most difficult for small $\tau$ values.

A review of the shapes of the $V_e(z)$ curves reveals that they are affected by the proximity of the aluminum adherend for epoxy thicknesses, $\tau$, up to approximately 30 μm. The dominant ripples in the $V_e(z)$ curves are generated through interference between reflected compression waves and leaky Rayleigh waves down to an epoxy thickness of $\tau = 14$ μm. These are the ripples with a periodicity of 8 to 10 μm, beginning immediately below the focal peak designated by FP in Figures 4(e) to 4(k). The other major feature is the aluminum interface peak marked by IP in Figures 4(b) to 4(i). The position of this peak moves towards the focal peak as the epoxy thickness, $\tau$,

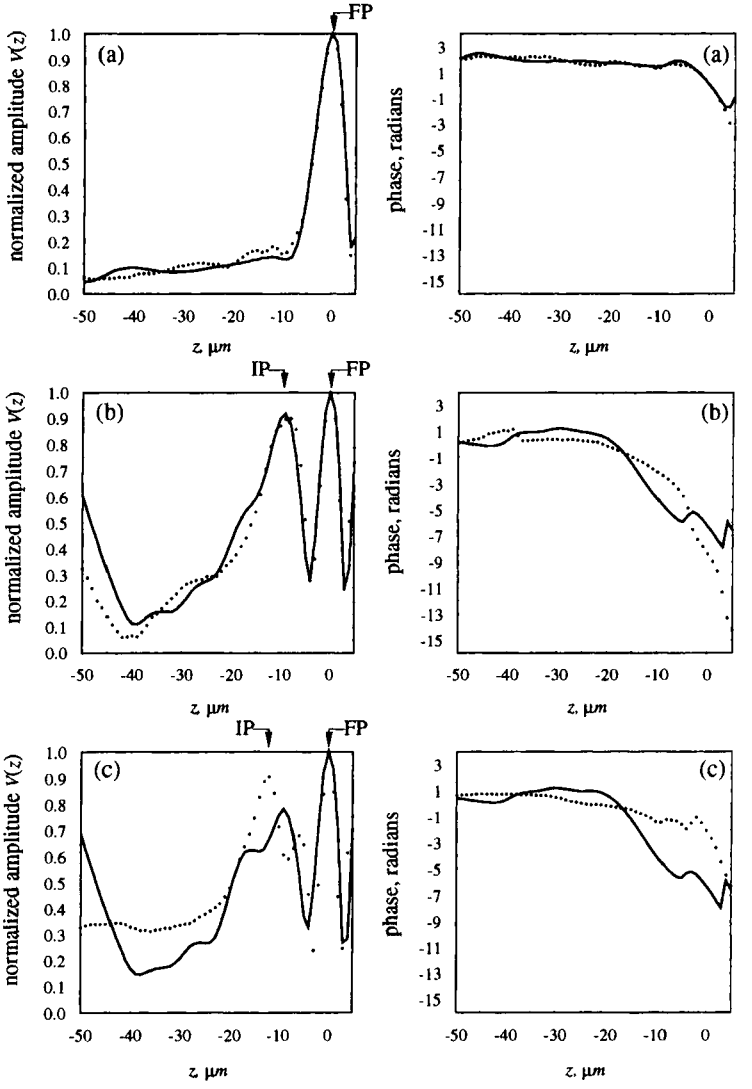


FIGURE 4 $V(z)$ curves for specimens with successively increasing thicknesses of remaining epoxy, $\tau$: (a) $\tau = 3.5\,\mu m$, (b) $\tau = 6.6\,\mu m$, (c) $\tau = 6.7\,\mu m$. Solid curves are calculated $V_t(z)$ and dotted ones are experimental $V_e(z)$, (d) $\tau = 8.4\,mm$, (e) $\tau = 14.0\,mm$, (f) $\tau = 17.8\,mm$, (g) $\tau = 20.3\,mm$, (h) $\tau = 23.0\,mm$, (i) $\tau = 26.0\,mm$, (j) $\tau = 32.2\,\mu m$, (k) $\tau = 41.7\,\mu m$.

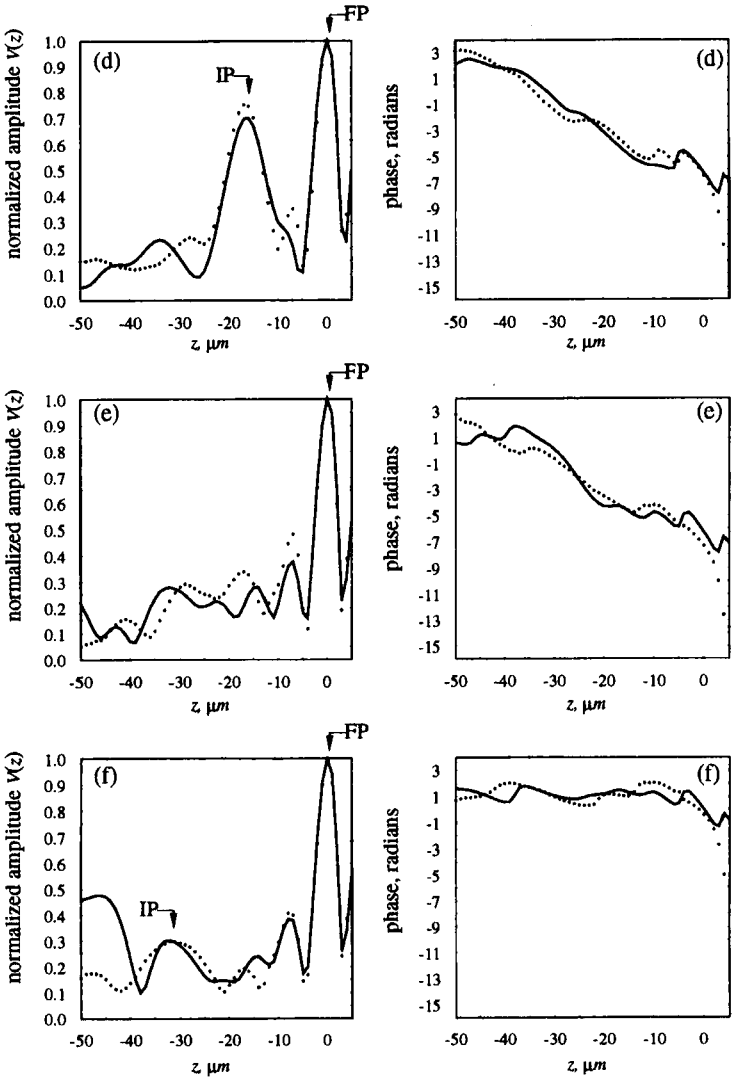


FIGURE 4 (Continued).

decreases. This peak has a simple ray explanation: the off-normal rays in the coupling fluid are converted to a set of shear wave and longitudinal wave rays in the epoxy layer which effectively form two new (aberrated) focal points inside the epoxy, (Fig. 5). The focal point

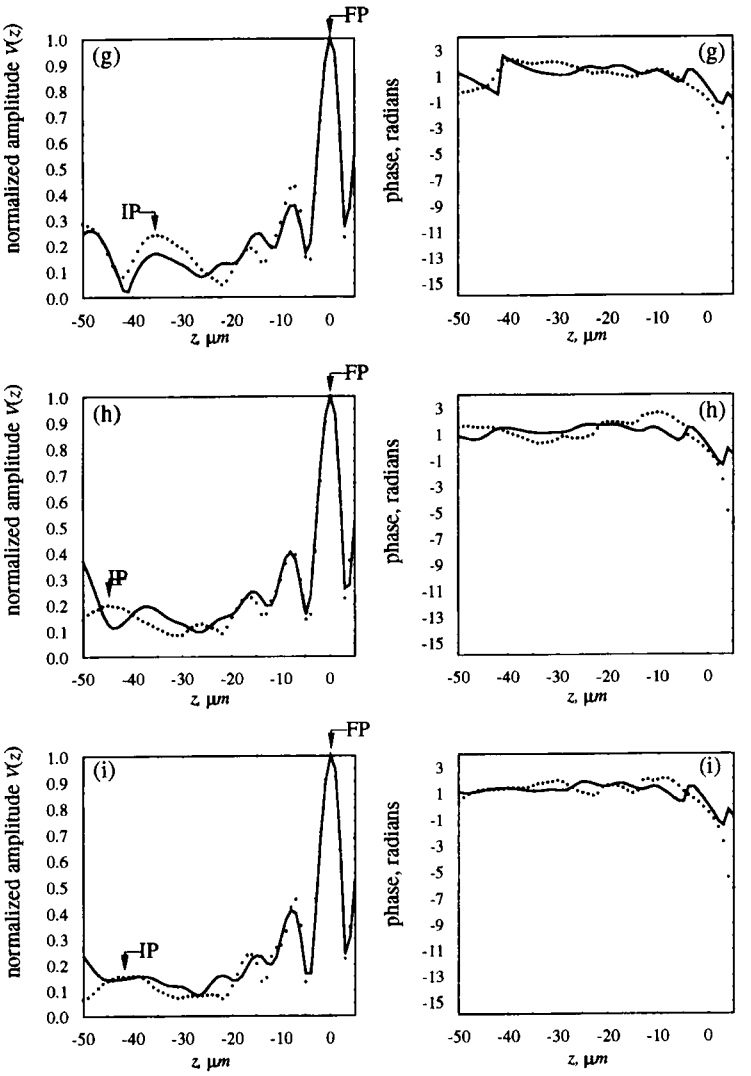


FIGURE 4 (Continued).

corresponding to the longitudinal waves is closer to the epoxy–couplant interface than that of the shear waves. At a certain $z$ range during the $V(z)$ scan, the shear wave focus reaches the highly reflective aluminum–epoxy interface and gives rise to the IP peak, which is not as sharp as the FP peak due to aberration effects. The longitudinal

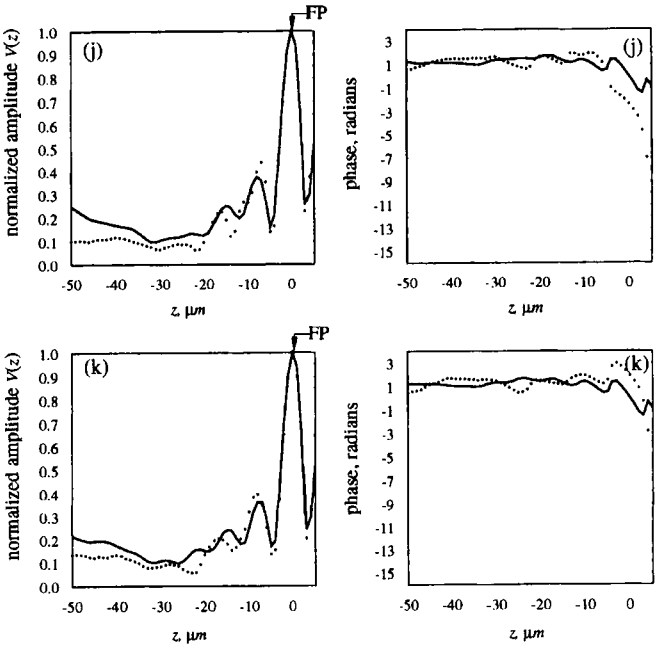


FIGURE 4 (Continued).

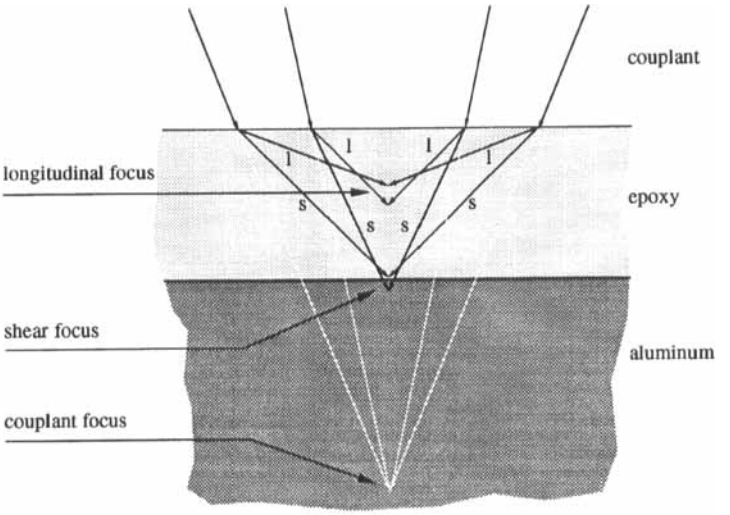


FIGURE 5 Focusing of the shear waves on the epoxy–aluminum interface.

focal point does not result in a distinct peak in the $V_e(z)$ curves for three reasons:

First, the difference between the longitudinal wave velocity in epoxy and the sound speed in the HCFC-225da couplant is larger than that corresponding to the shear wave velocity in epoxy, resulting in a more severe aberration.

Second, the impedance mismatch between the epoxy and the couplant is larger for longitudinal waves than for shear waves, resulting in a lower energy transmission coefficient for longitudinal waves.

Third, the effective lens aperture from which the focusing longitudinal rays originate is smaller (approximately 16° for longitudinal waves as opposed to 35° for shear waves), such that a much smaller energy source is available for the detection of the longitudinal wave focus at the epoxy-aluminum interface.

For the $V_e(z)$ curves of Figure 4(a), the epoxy thickness, $\tau$, is less than the penetration depth of the Rayleigh waves; therefore, these waves cannot propagate freely along the epoxy surface. Various types of surface and interface waves are possible, and the behavior of the $V_e(z)$ curve for this specimen cannot be explained in terms of a simple ray description.

Alternatively, the presence of various peaks in the $V_e(z)$ curves of Figure 4 can be explained from a field point of view. The transmitted wave field from the acoustic microscope probe consists of a range of plane wave components. These plane waves are reflected back towards the probe after interaction with the epoxy layer. Each reflected plane wave component is the result of interference between a specularly reflected wave from the epoxy surface and multiple reflections and transmissions from inside the epoxy layer. At the focal peak (FP), most of the reflected components arrive at the probe in phase, and give rise to the FP peak. The relative phase between the reflected plane wave components varies as the probe moves towards the specimen. These phase variations result in interference patterns which lead to various peaks in the $V_e(z)$ curves.

The results of the curve fitting procedure, as described in the Appendix, are represented by the solid curves $V_f(z)$ of Figures 4(a) to 4(k). The optimization procedure was very computationally intensive, and these fitted $V_f(z)$ curves took approximately 300 hours on a

166 MHz Pentium® personal computer to calculate. The importance of the attenuative nature of the epoxy in the calculations should be noted here, since no fit could be obtained without the inclusion of the attenuation factors in the multilayer model. The property distributions resulting in the above calculated $V_t(z)$ curves are presented in the next section.

All of the calculated $V_t(z)$ curves show the main features of the experimental $V_e(z)$ curves; *i.e.*, they show either the Rayleigh wave ripples or the shear wave focus on the epoxy–aluminum interface (designated by IP), or both. The fits to the experimental $V_e(z)$ curves for the 3.5 μm and 6.6 μm specimens are particularly good where the shapes of these $V(z)$ curves are the most sensitive to the interphase properties. However, Figure 4(c), corresponding to $\tau = 6.7\,\mu m$, does not show the double hump feature at the shear wave focus (IP).



### 4.2. Property Profiles

The property profiles resulting from the curve fitting procedure are presented in the solid curves of Figure 6. The key properties of interest are the longitudinal wave speed, $\nu_l$, the shear wave speed, $\nu_s$, and the density, $\rho$.

The material property profiles exhibit large gradients at values of $t$ less than 3 μm; however, the longitudinal and shear wave speeds still differ from those of the bulk even at distances as large as 40 microns form the interface, *i.e.*, 2 percent less than the bulk value for the shear wave speed, and 12 percent greater than the bulk value for the longitudinal wave speed. A comparison is made in Table I between the average material properties in the regions $0 < t < 5\,\mu m$ and $20\,\mu m < t < 40\,\mu m$. The zero to five micrometer region was chosen for this comparison because it represents the morphological extent of the interphase [22], as determined from microscopic studies. The region $20\,\mu m < t < 40\,\mu m$ was chosen since the property profiles show relatively little fluctuation in this area.

The Young's modulus, $E$, and shear modulus, $G$, profiles of Figure 7 were calculated from the velocity and density profiles of Figures 6(a), (b), and (c). First, the Lamé elastic constant profiles were calculated using the longitudinal and shear velocity profiles and the density profile. Then, the $E$ and $G$ profiles were calculated using the standard

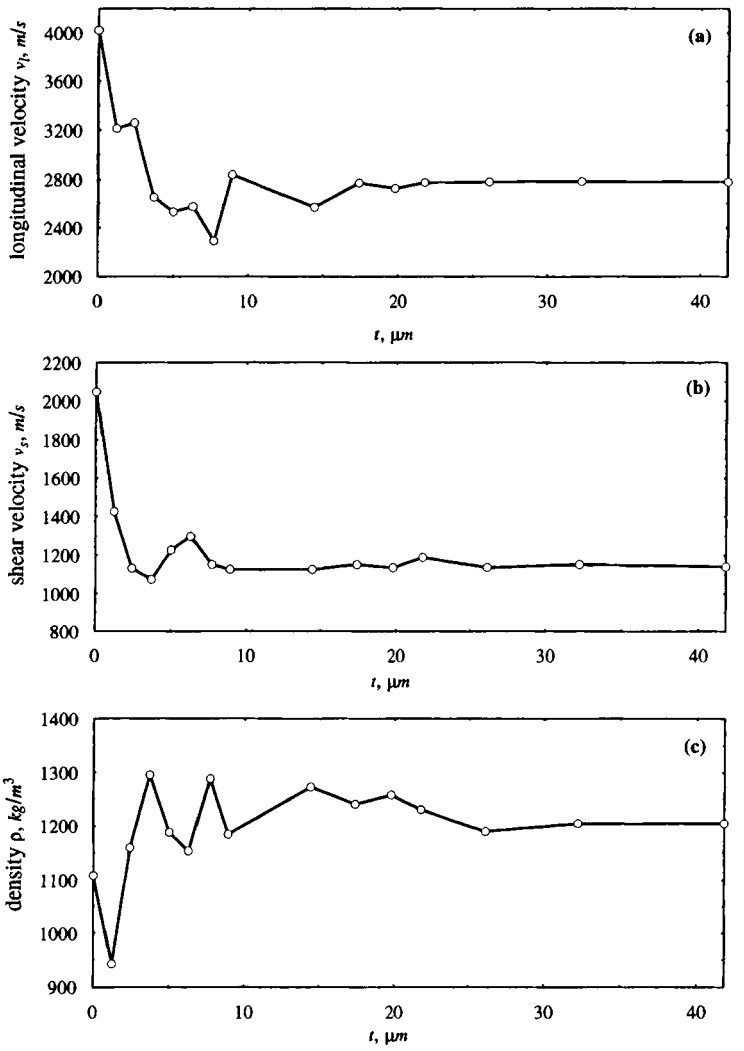


FIGURE 6 Property profiles across the interphase of EA9346-Aluminum adhesive system. The profile corresponds to the best fit curves of Figure 4: (a) velocity of longitudinal waves, (b) velocity of shear waves, (c) density.

relationships between these elastic constants and the Lamé elastic constants. The large gradients of $E$ and $G$ are evident for $t < 3\,\mu m$. Table I shows that the average values of $E$ and $G$ corresponding to the region $0 < t < 5\,\mu m$ are more than 20% greater than those for the

TABLE I A comparison of the average properties between two interfacial regions of epoxy EA 9346, based on acoustic microscopy measurements

| *Property* | $\nu_l$ *m/s* | $\nu_s$ *m/s* | $\rho$ *kg/m*$^3$ | *E GPa* | *G GPa* | $E_r$ *GPa* |
|---|---|---|---|---|---|---|
| average $0 < t < 5\,\mu m$ | 3086 | 1309 | 1140 | 5.52 | 2.01 | 6.44 |
| average $20 < t < 40\,\mu m$ | 2778 | 1150 | 1207 | 4.46 | 1.60 | 5.29 |
| % difference | 11.1% | 13.8% | −5.5% | 23.8% | 25.8% | 21.7% |

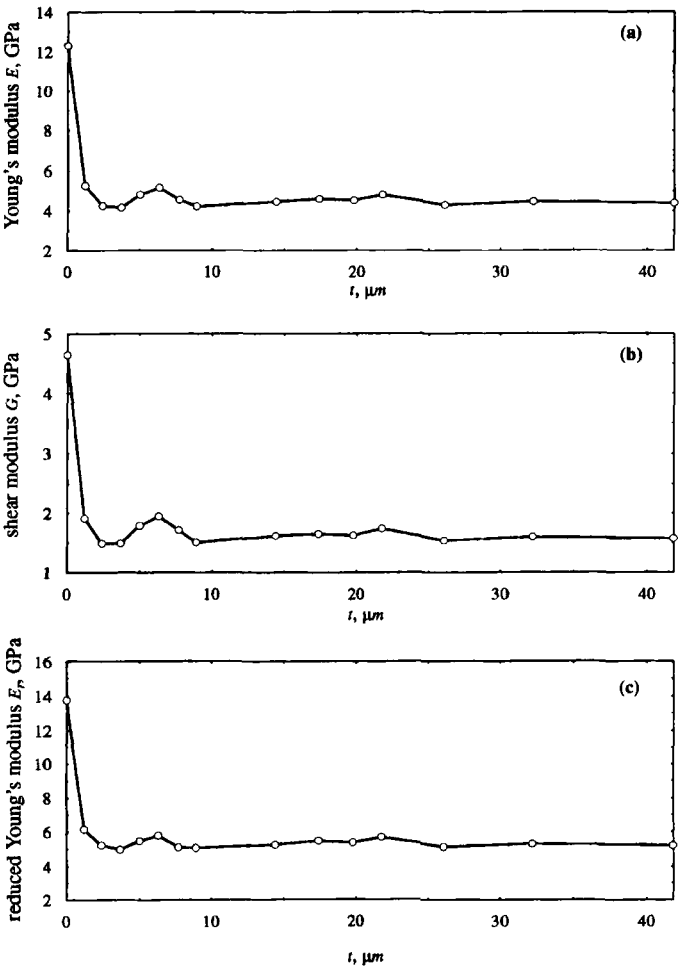


FIGURE 7 Property profiles across the interphase of EA9346-Aluminum adhesive system. The profile corresponds to the best fit curves of Figure 4: (a) Young's modulus, (b) shear modulus, (c) reduced Young's modulus.

TABLE II Summary of the experimentally-obtained values of $E_r$ for EA 9346 epoxy and the $E_r$ value calculated from the manufacturer's data sheet

| | *Acoustic microscope* | *Nanoindentation* | *Manufacturer's data* |
|---|---|---|---|
| Interphase $E_r$, GPa | 6.44 | 3.65 | – |
| Bulk $E_r$, GPa | 5.29 | 3.22 | 2.08 |

region corresponding to $t$ between 20 and 40 μm. In contrast to the differing profiles of the longitudinal velocity and the shear velocity, the $E$ profile has a shape similar to that of $G$. This occurs because Young's modulus, $E$, is a function of both the longitudinal and the shear speeds of sound; this is particularly true for plastics which have a relatively large Poisson's ratio.

The reduced modulus, $E_r = E/(1-\nu^2)$, profile is presented in Figure 7 for comparison with the nanoindentation results presented in [22]. The $E_r$ values from the acoustic microscope measurements were larger than those measured by the nanoindentation technique (Tab. II), although the trend of a rapid increase within a few microns of the aluminum was the same. The reasons for this difference are discussed in Section 5.

There are several sources of uncertainty in the results shown in Figures 6 and 7. One such source is the process of curve-fitting the data of Figure 4; a sensitivity analysis indicated that this led to an uncertainty of approximately $+/-3\%$ in the density and modulus profiles, but less than $+/-1\%$ in the shear and longitudinal velocity profiles. Signal averaging was employed to minimize effects of random electrical noise. SEM analysis indicated that there were significant point-to-point variations in the structure of the adhesive, particularly close to the aluminum. The large number of $V(z)$ curves considered in this study (12 curves on each of 11 specimens) would yield results representing an average profile of material properties, as functions of distance $t$ from the interface.

## 5. DISCUSSION

The curve-fitting procedure used in this work was a first attempt to solve the depth profiling problem with an acoustic microscope. In this

method, the convergence between $V_e(z)$ and $V_t(z)$ to a solution is not guaranteed, and the uniqueness of the answers cannot be proven theoretically; however, the large number of $V(z)$ curves used in the process introduces a large degree of redundancy in the fitted functions and reduces the possibility of uniqueness problems. This is supported by the observation that the calculated property profiles from the acoustic microscopy procedure are in qualitative agreement with the outcomes of the electron microscopic studies and the results of the nanoindentation technique [22].

The interphase thickness in a metal–adhesive system was previously believed to be in the nanometer range, and only a few studies indicated the existence of an interphase with a thickness of the order of microns. It may be questioned whether the acoustic microscope measurement and the curve-fitting procedure are sensitive enough to reveal differences between the interphase and bulk adhesive properties. The $V_t(z)$ curves of Figure 8 were calculated in order to investigate this question. These $V_t(z)$ curves were calculated with the assumption of homogeneous material properties throughout the epoxy right up to the adhesive/adherend interface. These constant property values were chosen by a curve-fitting procedure using only the experimental $V_e(z)$ curves corresponding to specimens with an epoxy thickness, $\tau$ larger than 20 μm. These experimental $V_e(z)$ curves are also presented in Figure 8. It is clear that these constant property $V_t(z)$ curves do not fit the data as well as the $V_t(z)$ curves of Figures 4(a) to (f), *i.e.*, a constant property profile cannot reproduce the shape of the experimental $V_e(z)$ curves.

The $E_r$ values obtained from acoustic microscopy, nanoindentation measurements, and manufacturer's data sheets for EA 9346 are summarized in Table II. Although the $E_r$ profiles of Figure 7, calculated using the acoustic microscope measurements, and the $E_r$ profiles from the nanoindentation tests reported in [22], show the same trend in the interphase region, the acoustic microscope results are larger. The $E_r$ values of Figure 7 are also greater than the values generally obtained for this adhesive by a simple tension test as presented in Table II (manufacturer's data). The reason for this is the difference in both the scale of loading and the speed of loading among the three cases. The applied deformations due to acoustic wave propagation in the epoxy occur at a very high frequency; viscous

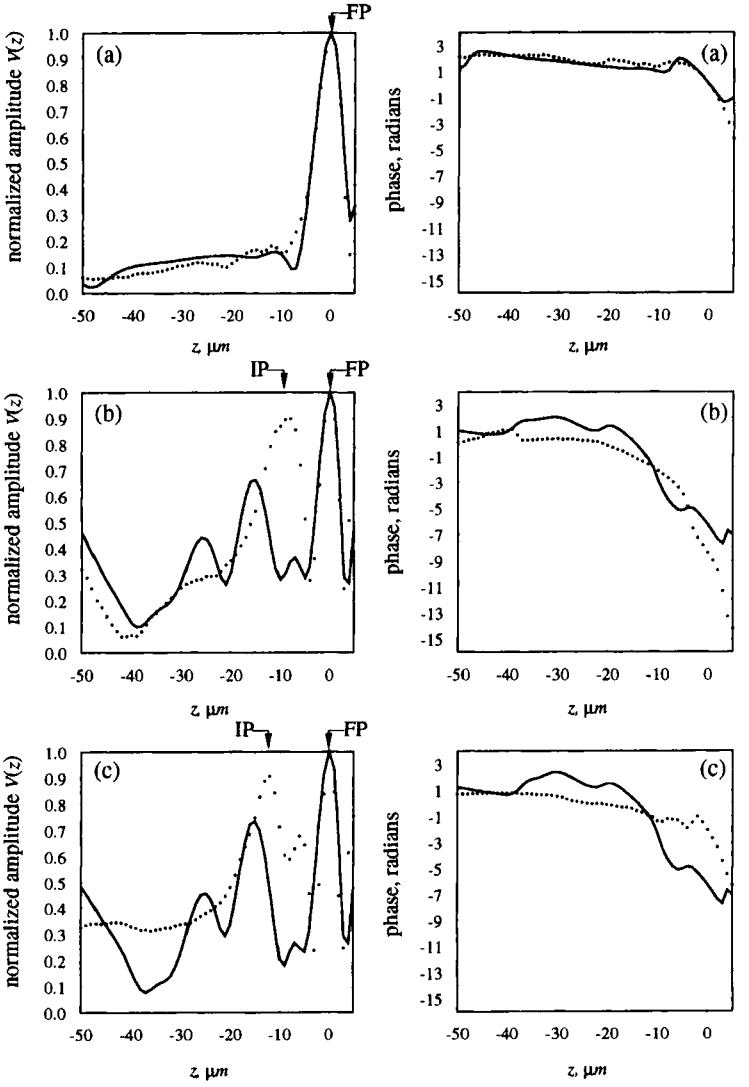


FIGURE 8 $V(z)$ curves for specimens with successively increasing thicknesses of epoxy, $\tau$: (a) $\tau = 3.5\,\mu m$, (b) $\tau = 6.5\,\mu m$, (c) $\tau = 6.7\,\mu m$. The solid curves are calculated $V_t(z)$ profiles, assuming constant material properties throughout the bulk adhesive and interphase. The dotted curves are the experimental $V_e(z)$ profiles. (d) $\tau = 8.4\,\mu m$, (e) $\tau = 14.0\,\mu m$, (f) $\tau = 17.8\,\mu m$.

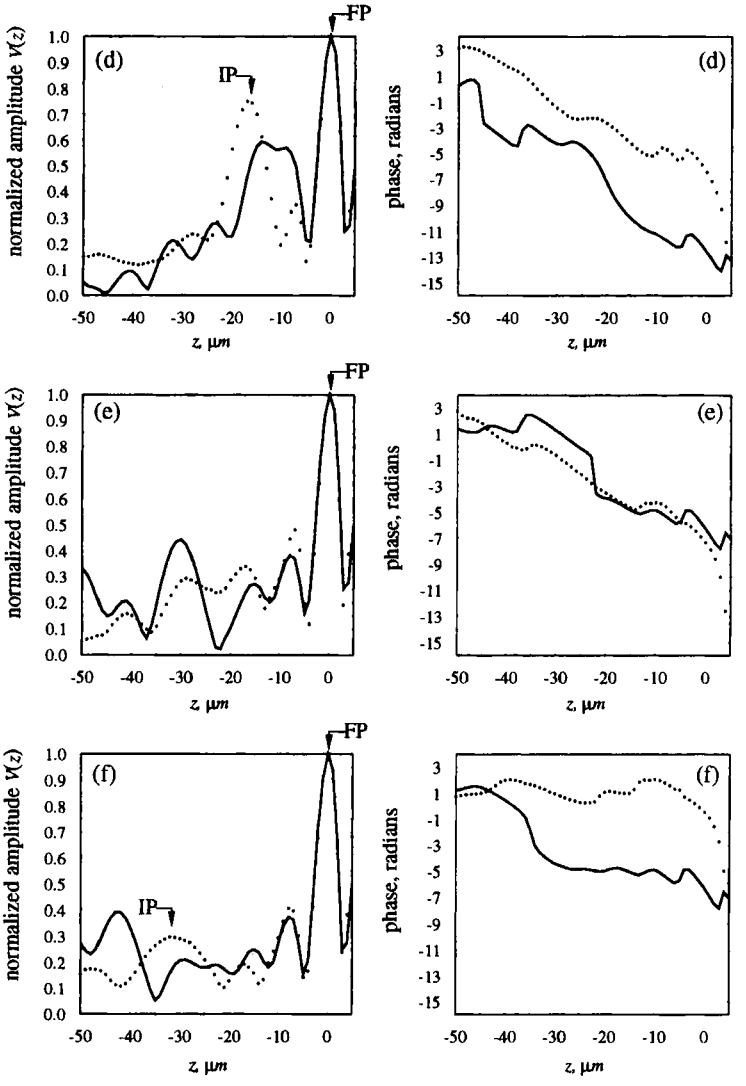


FIGURE 8 (Continued).

relaxation is, therefore, negligible and the apparent stiffness is relatively high. This is consistent with the observed increase of acoustic velocity with frequency in plastics up to a few MHz, with the velocity levelling off at higher frequencies. Such trends have been reported

previously for plastics, and are linked to a simple relaxation model of material response to deformation [29].

The nanoindentation test, although quasi-static, produces a localized deformation field in the epoxy which loads the polymer within individual clusters where the density of the cross-linking is high [30]. This raises the apparent stiffness value for the localized microscopic-scale loading in a nanoindentation test. By contrast, the large scale loading in a simple tension test moves the polymer clusters with respect to each other at locations where there is a relatively low cross-link density; this effect lowers the apparent stiffness values. These situations are schematically illustrated by the truss model of Figure 9.

Table I shows that the average value of $\rho$ for the region $0 < t < 5\,\mu m$ is 5.5% less than that of the region corresponding to $20\,\mu m < t < 40\,\mu m$. The reduced density of the interphase is consistent with the previously-observed absence of silica particles in this region [22]. However, this lack of silica particles can account for only half of the observed difference in the densities (based on an estimated density of pure epoxy of $p = 1.149\,g/cm^3$. This estimate was derived from the density of $p = 1.18\,g/cm^3$ for bulk epoxy assuming the maximum 5% (by weight) of silica particles of $p = 2.4\,g/cm^3$). The "excess" reduction in the density of the interphase may be attributed to differences in the polymer structure between the bulk and the interphase region.

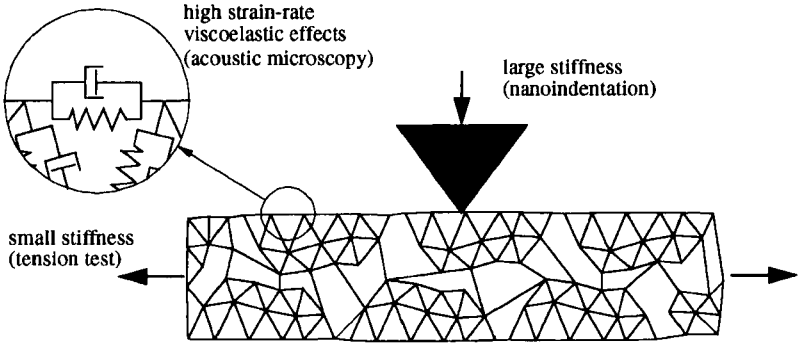


FIGURE 9 Simple truss model illustrating the difference in the loading scales for nanoindentation and tensile tests.

It has been shown in other epoxies that curing agents can adsorb preferentially to aluminum [14, 15]. The relatively large magnitude of the reduced modulus, $E_r$, of the interphase compared with the bulk adhesive, measured in both the present work and using nanoindentation in [22], may, therefore, be due to a higher local crosslink density. Racich and Koutsky [31] also attributed morphology changes in epoxy boundary layers to variations in the concentration of curing agents. Preferential curing from the aluminum also provides a possible explanation for the relative depletion of silica filler in the interphase, as reported for this same epoxy system in [22].

In comparing the present results with the literature, it is evident that the interphase properties display a wide range of behavior. The present interphase thickness was consistent with those reported in references [7, 8, 10], but less than that of [3] and [18]. The relative absence of silica particles in the interphase was also found in [10]. The large shear modulus in the interphase is opposite to the trend found in [4] and [18]; however, a larger modulus was measured in [6]. As mentioned above, relative to the bulk epoxy, the interphase has a higher modulus and a slightly lower density. This seemingly paradoxical result may be related to the observation that epoxy density can either increase or decrease with increasing crosslink density, although the changes are relatively much smaller than changes in other properties [30, 32].

The use of higher frequency acoustic microscopes would increase the spatial resolution of the measurements by reducing the ultrasonic wavelength. However, epoxies (and polymers in general) are highly attenuating, and the available signal power becomes a limiting factor; for a given transducer power output, the wave amplitude decreases as the frequency rises. In general, current acoustic microscopes lack sufficient power to probe polymers at significantly higher frequencies.

## 6. CONCLUSION

In this work, a first attempt was made to perform depth profiling of elastic properties with an acoustic microscope. A new acoustic microscope system was developed for this purpose [23]. This

microscope, which operated at a frequency of 250 MHz, utilized a new low-velocity ultrasonic couplant and an ultrasonic probe designed specifically for the characteristics of the new couplant.

A multiple curve-fitting procedure was used to infer the interphase property profiles from the measured $V_e(z)$ curves on specimens having a range of epoxy thicknesses. In this procedure, a large number of calculated $V_t(z)$ curves were fitted to the experimental ones simultaneously. The interphase regions were found to have a shear and longitudinal wave speeds which were, on average, 14% and 11% larger than those of the bulk adhesive, respectively. The average interphase density was 5.5% smaller than the bulk density.

## LIST OF SYMBOLS

| | |
|---|---|
| $E$ | Young's modulus (GPa) |
| $E_r$ | reduced Young's modulus, $E_r = E/(1-\nu^2)$ (GPa) |
| FP | focal point in acoustic microscope $V(z)$ profile |
| $G$ | shear modulus (GPa) |
| $R(\theta)$ | reflectance function |
| $t$ | perpendicular distance from epoxy-aluminum interface (mm) |
| $U$ | objective function representing distance between experimental and theoretical $V(z)$ profiles for 11 specimens |
| $\nu_l$ | longitudinal wave velocity (m/s) |
| $\nu_s$ | shear wave velocity (m/s) |
| $V(z)$ | voltage of received echo in an acoustic microscope, as a function of position $z$ (arbitrary) |
| $V_t(z)$ | calculated $V(z)$ function (arbitrary) |
| $V_e(z)$ | experimentally measured $V(z)$ function (arbitrary) |
| $W(z)$ | weighting function used in calculation of objective function $U$ |
| $w$ | bevel width on each of 11 specimens (see Fig. 2) (mm) |
| $z$ | position of acoustic microscope relative to focal peak (mm) |
| $z_{\max}$ | absolute $z$ value at maximum defocus of acoustic microscope |
| $zfp_t$ | $z$ value of first peak in $V_t(z)$ (mm) |
| $zfp_e$ | $z$ value of first peak in $V_e(z)$ (mm) |
| $\alpha_l$ | attenuation factor for longitudinal waves (Np/mm) |
| $\alpha_s$ | attenuation factor for shear waves (Np/mm) |
| $\rho$ | density (kg/m$^3$) |

$\tau_i$ thickness of epoxy remaining on a specimen, $i = 1, 2, \ldots, 11$ (mm)

$\theta$ angle of incidence of a plane wave on a solid from a liquid (radians)

$\nu$ Poisson's ratio

## Acknowledgment

The authors gratefully acknowledge the financial support of the Natural Sciences and Engineering Research Council of Canada, grant # CPG0163928, and the scholarship program of the Ministry of Culture and Higher Education of Iran.

## References

[1] Kinloch, A. J., In: *Durability of Structural Adhesives* (Elsevier Applied Science, Amsterdam, 1983), Chap. 1, pp. 1–39.
[2] Sharpe, L. H., *J. Adhesion* **4**, 51–64 (1972).
[3] Cuthrell, R. E., *J. Appl. Polymer Sci.* **11**, 949–952 (1967).
[4] Williams, J. C., Donnellan, M. E., James, M. R. and Morris, W. C., *Proceedings of the Mat. Res. Soc.* **170**, 285–290 (1990).
[5] Skurlis, T. P. and McCullough, R. L., *Proceedings of the American Society for Composites, ASC* (Technomic, Laucaster, PA, 1994), pp. 218–226.
[6] Al-Moussawi, H., Drown, E. K. and Drzal, L. T., *Polymer Composites* **14**, 195–200 (1993).
[7] Possart, W., *Int. J. Adhesion and Adhesives* **8**, 77–83 (1988).
[8] Cognard, J., *Int. J. Adhesion and Adhesives* **11**, 114–116 (1991).
[9] Hahn, O. and Koetting, G., *Schweissen und Schneiden* **5**, 137–141 (1985).
[10] Crompton, S., *J. Mater. Sci.* **24**, 1575–1581 (1989).
[11] Crompton, S. and Andrews, P. R., *Proceedings of 10th RISO Intl. Symp. on Metallurgy and Materials Science* pp. 307–311 (1989).
[12] Spigel, B. and Roy, S., *J. Adhesion* **47**, 151–163 (1994).
[13] Ramakrishnan, N., De, A. K. and Suryanarayan, S., *J. Test. Eval.* **10**, 192–198 (1982).
[14] Nakamae, K., Nishino, T., Airu, X. and Asaoka, S., *Int. J. Adhesion and Adhesives* **15**, 15–20 (1995).
[15] Affrosman, S., McAllister, J. M. R., Pethrick, R. A., Thomson, B., Brown, N. M. D. and Meenan, B. J., *Polym. Surf. Interf.* **1**, 107 (1987).
[16] Wang, S. and Garton, A., *Proceedings of the ACS Division of Polymeric Materials Science and Engineering* **60**, 805–809 (1989).
[17] Maguire, J. F., Talley, P. L. and Lupkowski, M., *J. Adhesion* **45**, 269–290 (1994).
[18] Knollman, G. C., *Int. J. Adhesion and Adhesives* **5**, 137–141 (1985).
[19] Cognard, J., Sattish, S., Kullick, A. and Gremond, G., *J. Adhesion* **32**, 45–49 (1990).
[20] Verma, Y., Ananda, A. A., Wilkinson, S. P. and Smith, T. B., In: *Proceedings of Review of Progress in QNDE* Vol. 13, Thompson, D. O. and Chimenti, D. E. Eds. (Plenum Press, NY, 1994), p. 1498.

[21] Sklar, Z. and Briggs, G. A. D., In: *Proceedings of Review of Progress in QNDE* Vol. 14, Thompson, D. O. and Chimenti, D. E. Eds. (Plenum Press, NY, 1995), pp. 1441–1449.
[22] Safavi-Ardebili, V., Spelt, J. K. and Sinclair, A. N., *J. Adhesion* **62**, 93–111 (1997).
[23] Safavi-Ardebili, V., Sinclair, A. N. and Spelt, J. K., *Proceedings of 1996 IEEE Ultrasonics Symp.* Levy, M., Schneider, S. C. and McAvoy, B. R. Eds. (IEEE, NY, 1996), pp. 807–810.
[24] Safavi-Ardebili, V., Sinclair, A. N. and Spelt, J. K., *IEEE Trans Ultrasonics, Ferroelectrics, and Frequency Control* **44**, 102–107 (1997).
[25] ASTM D2651-79 Method G (American Society for Testing and Materials, Philadelphia, PA, 1984).
[26] Safavi-Ardebili, V., *Ph.D. Thesis* University of Toronto (1998).
[27] Achenbach, J. D., Kim, J. G. and Lee, Y. C., In: *Advances in Acoustic Microscopy* Vol. 1, Briggs, A. Ed. (Plenum Press, New York, 1995), pp. 153–208.
[28] Yu, Z. and Boseck, S., *Optik* **88**, 73 (1991).
[29] McCammond, D., Sinclair, A. N. and Sinclair, L. A., In: *Cyclic Deformation, Fracture, and Nondestructive Evaluation of Advanced Materials* Mitchell M. R. and Buck, O. Eds., ASTM **STP 1157**, 151–170 (1992).
[30] Stevens, V. G. C., In: *Structural Adhesives: Developments in Resins and Polymers* Kinloch, A. J. Ed. (Elsevier Applied Science, New York, 1986), p. 201.
[31] Racich, J. L. and Koutsky, J. A., *Proceedings of the ACS Symposium on Chemistry and Properties of Crosslinked Polymers* San Francisco, Labana, S. S. Ed. pp. 303–323 (1976).
[32] Selby, K. and Miller, L. E., *J. Mat. Sci.* **10**, 12–24 (1975).
[33] Levesque, D. and Piche, L., *J. Acoust. Soc. Am.* **92**, 452–467 (1992).



## 8. APPENDIX: CALCULATION OF INTERPHASE MATERIAL PROPERTY PROFILES

Depth profiles of five material properties were sought for the interphase: the speed of the longitudinal wave, $\nu_l$, the speed of the shear wave, $\nu_s$, the attenuation factor for longitudinal wave, $\alpha_l$, the attenuation factor for shear wave, $\alpha_s$, and the density, $\rho$. These were to be determined such that the experimental $V(z)$ curves would be as close as possible to those measured by acoustic microscopy. The first step was to calculate the reflectance function, $R(\theta)$, for each specimen. For a given set of five property functions, this was handled by modelling the epoxy adjacent to the aluminum as a multilayer medium where each layer was assigned a homogenized, spatially-averaged set of the five material constants, $\nu_l$, $\nu_s$, $\alpha_l$, $\alpha_s$, and $\rho$. Although the material properties vary continuously across the interphase as a function of the distance, $t$, from the aluminum, a number of test runs showed that if the model's property jumps from one layer to the next were kept below eight percent, the discretization of the interphase had a negligible effect

on the reflectance function, $R(\theta)$. The resulting multilayer model was solved for $R(\theta)$ by a variation of the standard transfer matrix method [33]. The use of a modified method was necessary in order to avoid numerical instabilities which resulted from the presence of the surface waves and the attenuative nature of epoxy at high frequencies.

Another step towards the numerical calculation of $V(z)$ curves was the calibration of the lens; *i.e.*, finding a good approximation to the pupil function of the lens. The calibration was achieved by collecting $V(z)$ curves on a glass specimen with well-known mechanical properties and then fitting the calculated $V(z)$ curves to the experimental ones by adjusting the probe's geometrical parameters in the numerical model within the probe's fabrication tolerances.

No *a priori* constraints were placed on the type of function of $t$ chosen to describe the epoxy property profiles. It was deduced from the microscopic studies that the transition between the bulk and the interphase was gradual and continuous [22]. However, to facilitate the numerical work, each of the five material property functions (profiles) was "digitized" by representing it by a finite number of property values, corresponding to various distances, $t$, from the interface. The intermediate values of the property could then be calculated by linear interpolation between these "defining points". In order to simplify the calculations, the values of $t$ corresponding to these "defining points" were chosen to be close to the thicknesses, $\tau$, of the residual microtomed epoxy on the eleven specimens. A number of additional defining points were chosen for the region close to the interface since larger gradients of properties were anticipated in this region (Fig. 3). As a result of these considerations, 15 defining points were chosen for each of the material properties. The $V(z)$ profile calculated based on these digitized material property functions was labelled $V_t(z)$.

The procedure for matching $V_t(z)$ to the experimental profile, labelled $V_e(z)$, required the minimization of an objective function. The choice of the objective function was critical because of three factors: First, the $V(z)$ curve is a complex curve and both the magnitude and phase components should be matched. Under ideal conditions, where $V_e(z)$ contains negligible experimental error, a good fit between the magnitudes of $V_e(z)$ and $V_t(z)$ will automatically provide a simultaneous fit to the phase. In a realistic situation, however, this may not happen, and the objective function should have some components

representing the complex numbers in the $V(z)$ curves. Second, the magnitude of the $V(z)$ curve is a semi-periodic function which leads to a large number of local minima for a simple sum-of-squares objective function. A term representing the difference in the $z$ values corresponding to $V_e(z)$ and $V_t(z)$ for the first peak below the focal peak was included in the objective function. Third, it was anticipated that the $V_e(z)$ curve would be more accurate for regions of $z$ close to the focal point due to the larger signal-to-noise ratio. A weight factor, $W(z)$, was incorporated in the objective function which had a unit value at the focal point and decreased linearly with increasing distance from the focal point on the $V(z)$ curve.

The above considerations led to an objective function with three components:

$$U = 5 \sum_{11 \text{ specimens}} \left( \frac{\sum_{\text{all } z} W(z)|V_t(z) - V_e(z)|}{\sum_{\text{all } z} |V_e(z)|} \right) + 200 \sum_{11 \text{ specimens}} \left( \frac{\sum_{\text{all } z} [W(z)(|V_t(z)| - |V_e(z)|)]^2}{\sum_{\text{all } z} |V_e(z)|} \right) + \sum_{11 \text{ specimens}} [(zfp_t - zfp_e) \times 10^5]^2 \quad (1)$$

$V_t(z)$ is dependent on the input material property profiles. $V_e(z)$ was determined by averaging the experimental $V(z)$ profiles as described earlier for each of the eleven specimens. The numerical factors preceding the summation symbols were chosen by trial and error, and served to equalize approximately the relative weights of the three components of the objective function. The parameters $zfp_t$ and $zfp_e$ are the $z$ values of the first peak in the calculated and experimental $V(z)$ curves, respectively, and are located below the focal peak. $W(z)$ is defined as:

$$W(z) = \frac{z_{\max} - |z|}{z_{\max}} \quad (2)$$

where $z = 0$ is located at the focal peak and $z_{\max}$ is the absolute $z$ value of the largest defocus.

The objective function, $U$, defined by Eq. (1) is a function of the material properties at the fifteen "defining points". These property

values were the major optimization parameters for which initial values were needed in order to begin the optimization procedure. The initial property values at the defining points corresponding to $t > 10\ \mu m$ were found by taking a single value for each property (*i.e.*, 5 variables, each corresponding to the bulk value) and optimizing each value to minimize the objective function for the corresponding $V_e(z)$ curves. This method did not work for the defining points near the interface ($0\ \mu m \leq t < 10\ \mu m$). The initial estimates of property values corresponding to the points for which $t < 10\ \mu m$ were obtained by trial and error, to yield a reasonable match between $V_e(z)$ and $V_t(z)$.

The procedure outlined in the preceding paragraphs led to a preliminary set of material property values at the defining points for which the corresponding $V_t(z)$ curves were qualitatively similar to their experimental counterparts. These preliminary property values were then optimized in a step-by-step fashion based on the objective function of Eq. (1). The optimization process was designed to avoid instabilities without leading to excessive computational time.

It is noted that the objective function, $U$, is indirectly a function of the epoxy thickness, $\tau$, on each of the eleven specimens. Although these thicknesses were determined by sectioning through the specimens, they were subject to minor measurement errors. Therefore, in the final step of the optimization procedure, all of the property values and specimen thicknesses were "fine tuned" by taking all of them as the optimization parameters. Eighty-six parameters were involved in the final optimization, *i.e.*, 5 material properties at each of the 15 defining points, plus 11 epoxy thicknesses, $\tau$, of the experimental specimens.